Cell Reports

Article

Gut microbiota-mediated secondary bile acids regulate dendritic cells to attenuate autoimmune uveitis through TGR5 signaling

Graphical abstract

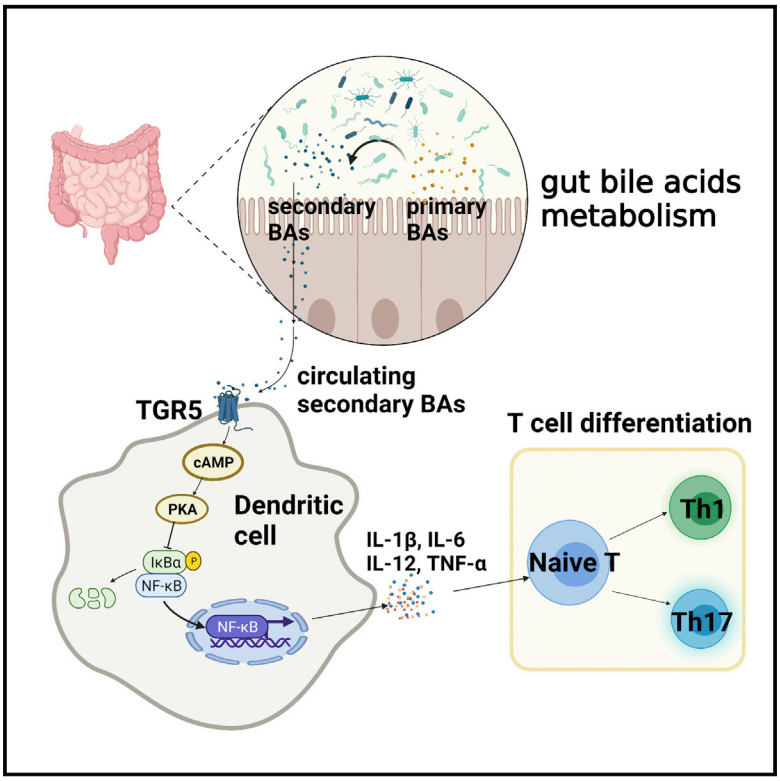

Authors

Jianping Hu, Chaokui Wang, Xinyue Huang, ..., Qingfeng Cao, Xingsheng Ye, Hong Li

Correspondence

lihongcqmu@163.com

In brief

Hu et al. reveal that gut microbiota-related dysmetabolism of bile acids is involved in the development of experimental autoimmune uveitis (EAU). Secondary bile acids are reduced in the feces and serum of EAU mice. Secondary bile acids regulate function of dendritic cells via the TGR5-cAMP-PKA pathway in EAU mice.

Highlights

- Secondary bile acids reduce severity of experimental autoimmine uveitis (EAU) in mice
- Altered bile acids are correlated with gut microbiota composition in EAU mice
- Deoxycholic acid regulates the function of DCs via the TGR5-cAMP-PKA pathway

Hu et al., 2021, Cell Reports *36*, 109726
September 21, 2021
https://doi.org/10.1016/j.celrep.2021.109726

CellPress

Cell Reports

CellPress
OPEN ACCESS

Article

Gut microbiota-mediated secondary bile acids regulate dendritic cells to attenuate autoimmune uveitis through TGR5 signaling

Jianping Hu,[1] Chaokui Wang,[1] Xinyue Huang,[1] Shenglan Yi,[1] Su Pan,[1] Yiting Zhang,[1] Gangxiang Yuan,[1] Qingfeng Cao,[1] Xingsheng Ye,[1] and Hong Li[1,2,*]

[1]The First Affiliated Hospital of Chongqing Medical University, Chongqing Key Laboratory of Ophthalmology, Chongqing Eye Institute, and Chongqing Branch of National Clinical Research Center for Ocular Diseases, Chongqing, P.R. China

[2]Lead contact

*Correspondence: lihongcqmu@163.com

https://doi.org/10.1016/j.celrep.2021.109726

SUMMARY

Gut microbiota-mediated secondary bile acids (BAs) play an important role in energy balance and host metabolism via G protein-coupled receptors and/or nuclear receptors. Emerging evidence suggests that BAs are important for maintaining innate immune responses via these receptors. However, the effect of BAs on autoimmune uveitis is still unknown. Here, we demonstrate decreased microbiota-related secondary BA concentration in feces and serum of animals with experimental autoimmune uveitis (EAU). Restoration of the gut BAs pool attenuates severity of EAU in association with inhibition of nuclear factor κB (NF-κB)-related pro-inflammatory cytokines in dendritic cells (DCs). TGR5 deficiency partially reverses the inhibitory effect of deoxycholic acid (DCA) on DCs. TGR5 signaling also inhibits NF-κB activation via the cyclic AMP (cAMP)-protein kinase A (PKA) pathway in DCs. Additionally, both DCA and TGR5 agonists inhibit human monocyte-derived DC activation. Taken together, our results suggest that BA metabolism plays an important role in adaptive immune responses and might be a therapeutic target in autoimmune uveitis.

INTRODUCTION

Uveitis is an intraocular inflammatory disease that may cause severe visual impairment (Miserocchi et al., 2013). Uveitis is currently treated with corticosteroids and immunosuppressive agents, but despite this therapy many eyes still go blind. Therefore, there is an ongoing search to elucidate the mechanisms involved in the pathogenesis of uveitis, which might lead to the discovery of potential therapeutic targets.

Recent studies showed that dysbiosis of the gut microbiome might play an important role in modulating immune homeostasis in clinical uveitis entities such as Behçet's disease (BD), Vogt-Koyanagi-Harada (VKH) disease, and acute anterior uveitis (AAU), but also in a model of experimental autoimmune uveitis (EAU) (Huang et al., 2018a; Janowitz et al., 2019; Ye et al., 2018, 2020). Transplantation of feces from clinically active BD uveitis patients to mice was shown to worsen EAU in these animals (Ye et al., 2018). An altered composition of the gut microbiota has recently not only been observed in uveitis, but also in many other autoimmune/inflammatory diseases (Bhargava et al., 2020; Huang et al., 2018a; Nakamura et al., 2016; Stoll et al., 2014; Tremlett et al., 2016; Ye et al., 2018). How gut microbiota composition affects immune regulation is not yet clear, and secondary effects, such as a microbiota-associated influence on bile acid composition, have only scarcely been investigated (Abdollahi-Roodsaz et al., 2016; Dart, 2018; Shapiro et al., 2018; Taylor and Green, 2018).

Bile acids are produced in the liver and are metabolized by enzymes derived from intestinal bacteria, and they have been shown to be involved in the control of the immune system (Fiorucci et al., 2018; Ye et al., 2018). Research on the immunoregulatory effects of bile acids has mainly focused on their control of innate immunity (Fiorucci et al., 2018). Recent studies found that a gut microbiota-related dysmetabolism of bile acids was associated with several inflammatory autoimmune diseases such as inflammatory bowel disease (IBD) (Duboc et al., 2013) and type 1 diabetes (T1D) (Mooranian et al., 2018). A role for bile acid composition in the pathogenesis of uveitis has not yet been reported and was therefore the subject of the study presented here.

In this study, we tested bile acids and gut microbiota composition in an animal model of uveitis (EAU). We found that gut microbiota-related secondary bile acids suppress the severity of EAU and show that this effect may be mediated via a TGR5-induced inhibition of dendritic cell (DC) activation.

RESULTS

Altered bile acids and gut microbiota composition in the feces of EAU mice

Current studies have indicated that a dysregulation of gut microbiota plays a critical role in the development and the progression of several autoimmune diseases, including uveitis (Wu et al.,

2020; Ye et al., 2018). However, how the gut microbiota plays its effect on uveitis is still not well clarified. First, gut microbiota composition in the feces of EAU mice was tested by 16S rDNA sequencing. A significant change was found between EAU and control mice at the phylum and genus levels (Figures S1A). The Chao1 and Shannon indexes were decreased and the Simpson index was increased, showing a downregulation of microflora richness and diversity in the feces of EAU mice (Figure S1B). Additionally, the principal-component analysis (PCA) and principal coordinate analysis (PCoA) score plots revealed a clear difference between EAU mice and healthy controls (Figure S1C). We further used the linear discriminant analysis (LDA) effect size (LEfSe) tool to characterize the change of the gut microbiota in EAU mice. The result showed that Ruminococcaceae (Firmicutes), Lachnospiraceae (Firmicutes), and Eggerthellaceae (Actinobacteria) were enriched in controls, whereas Prevotellaceae (Bacteroidetes) was enriched in EAU mice (Figures 1D and 1E).

Recent studies have reported that Ruminococcaceae and Lachnospiraceae might exhibit a bile acid-inducible 7α-dehydroxylation that converts primary bile acids into secondary bile acids (Just et al., 2018; Vital et al., 2019). To investigate whether bile acid composition was involved in the development of autoimmune uveitis, we collected feces from C57BL/6J mice on day 14 after being immunized with $IRBP_{651–670}$ and complete Freund's adjuvant (CFA). Fecal bile acid composition was tested by liquid chromatography-mass spectrometry (LC-MS). Total secondary bile acids and the secondary bile acids/primary bile acids ratio were found to be decreased in the EAU group (Figures 1B and 1C). Four secondary bile acids and two primary bile acids were decreased (Figure 1A). We further performed Spearman correlation tests between microbial taxonomic composition at the genus level (LDA > 2, $p < 0.05$) and altered bile acids ($p < 0.05$). A total of 47 genera (13 enriched and 34 depleted in feces of EAU mice) and six bile acids were significantly associated with at least one potential interaction. Deoxycholic acid (DCA) was significantly correlated with 28 genera, including 8 genera belonging to Lachnospiraceae and 8 genera belonging to Ruminococcaceae (Figures 1F and 1G).

Gut-mediated secondary bile acids suppress the clinical severity of EAU

The above results indicated that dysmetabolism of gut-mediated secondary bile acids was involved in the development of EAU mice. To further study how gut secondary bile acids affect the development of autoimmune uveitis, we tested the level of circulating bile acids of EAU mice. We found that secondary bile acids were decreased in the serum of EAU mice, including DCA and another four secondary bile acids (Figures S2A–S2C). Furthermore, fecal bile acid concentration was positively correlated with circulating bile acid level (Figure S2D). We next immediately fed mice with various diets containing either DCA, cholic acid (CA), lithocholic acid (LCA), or chenodeoxycholic acid (CDCA), and controls received a normal diet (ND) after inducing EAU. The results showed that DCA and LCA, but not CA and CDCA, significantly suppressed the progression of EAU mice in the clinic with a reduction of spleen weight (Figures 2A, 2B, and S5B). The diets did not affect body weight, blood glucose, and plasma ALT level (Figures S5A and S5C). The histological scores of EAU mice on day 14 after immunization were decreased by DCA and LCA (Figures 2A and 2B). Additionally, we found that the percentage of T helper (Th)1 and Th17 cells in spleen was decreased by LCA and DCA (Figures 2C and 2E). LCA and DCA also significantly decreased the frequency of splenic $CD11c^+$major histocompatibility complex class II (MHC class II)^{high} DCs (Figures 2D and 2F).

Bile acids have been shown to influence the composition of the gut microbiota (Jia et al., 2018). We pretreated mice with antibiotics (ABs) for 7 days to delete the existing gut flora and then fed mice with an LCA or DCA diet. EAU was induced by IRBP immunization, and both LCA and DCA reduced the severity of EAU, as shown by the lower clinical histological scores with a reduction of spleen weight (Figures S3A–S3D and S5E). Antibiotics also had no effect on body weight and blood glucose (Figure S5D). Analysis of splenic cells showed inhibited Th1 and Th17 differentiation and $CD11c^+$MHC class II^{high} DC activation as compared with the antibiotic pretreatment group (Figures S3E–S3H). Interestingly, antibiotics also significantly attenuated the severity of EAU and decreased the proportion of Th1 and Th17 cells in the spleen (Figures S3A–S3D, S3G, and S3H), but did not inhibit $CD11c^+$MHC class II^{high} DC activation (Figures S3E and S3F).

Clostridium scindens has been reported to be depleted in feces of BD and AAU patients and has been shown to convert primary bile acids into secondary bile acids (Huang et al., 2018a; Ye et al., 2018). We found that *C. scindens* was depleted in feces of EAU mice (Figure S4A). Therefore, we colonized mice with *C. scindens* and then immunized them with $IRBP_{651–670}$. Our results showed that *C. scindens* was significantly enriched and that it increased the proportion of secondary bile acids in mice feces and serum (Figures S4A–S4E). In addition, the proportion of secondary bile acids in serum and feces was positively correlated with the level of fecal *C. scindens* (Figures S4F and S4G). We next found that *C. scindens* transplantation significantly inhibited clinical, histological scores and spleen weight in EAU mice (Figures 2G, 2H, and S6G), but it had no effect on body weight and blood glucose (Figure S5F). Additionally, it also reduced the proportion of Th1 cells, Th17 cells, and $CD11c^+$MHC class II^{high} DCs in the spleen of EAU mice (Figures 2I–2L).

Secondary bile acid regulates the function of DCs *in vivo* and *in vitro*

The results shown above suggested that secondary bile acids regulate $CD11c^+$MHC class II^{high} DC activation in EAU mice. DCs are professional antigen-presenting cells critical for the function of the adaptive immune systems via their ability to prime naive T cells and thus play a key role in maintaining immune homeostasis and tolerance (Allenspach et al., 2008). We developed bone marrow-derived DCs (BMDCs) to evaluate the effects of secondary bile acids on DCs *in vitro*. We found that DCA significantly reduced the secretion of interleukin (IL)-1β, IL-6, tumor necrosis factor (TNF)-α, and IL-12p70 by lipopolysaccharide (LPS)-primed BMDCs in a dose-dependent manner (Figure 3A). Additionally, DCA also inhibited the expression of co-stimulatory molecules such as CD40, CD80, CD86, and MHC class II (Figures 3B and 3C). To examine the effect of DCA on the role of BMDCs on

CellPress
OPEN ACCESS

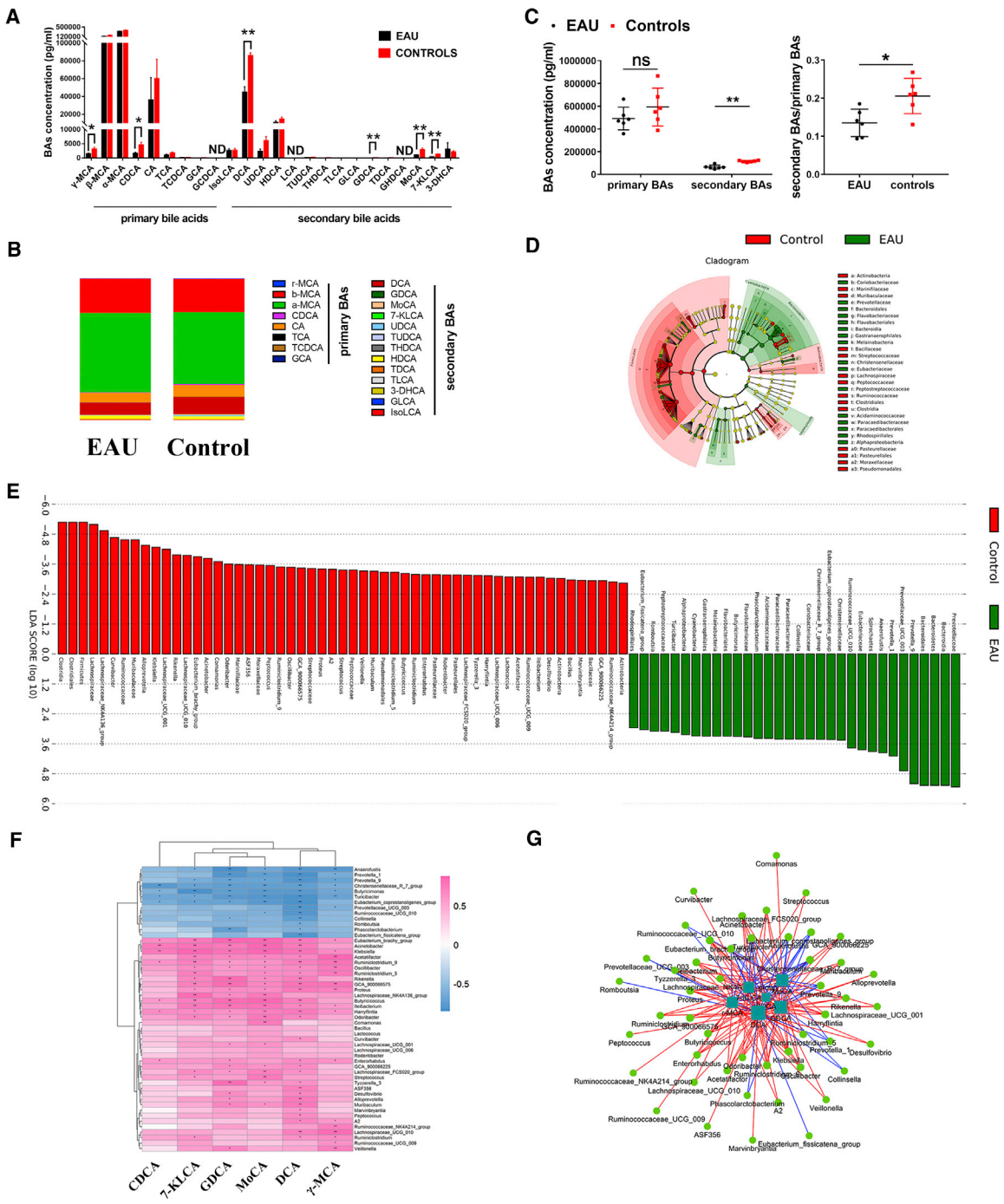

Figure 1. Altered bile acids (BAs) and gut microbiota composition in the feces of EAU mice

C57BL/6J mice were immunized by $IRBP_{651–670}$ and CFA to induce EAU, and feces was collected on the 14th day after immunization at the peak of their uveitis (n = 6 per group). BAs in the feces of EAU mice and controls were tested by LC-MS.

(A) Levels of fecal BAs in EAU mice and controls.

(B) Fecal BA composition in EAU mice and controls.

(C) Fecal primary BAs, secondary BAs, and the ratio of secondary BAs/primary BAs compared between EAU mice and controls.

(D) The differentially abundant taxonomic clades with a linear discriminant analysis (LDA) score >2.0 among cases with a p value <0.05.

(E) LDA effect size (LefSe) analysis in EAU mice (green) and controls (red).

(F and G) Heatmap (F) and network (G) of positive (red) and opposite (blue) correlation between six BAs and 41 genera.

Data are shown as mean ± SD. An unpaired t test, Mann-Whitney U test, and Spearman correlation analysis were used. *p < 0.05, **p < 0.01; ns, not significant (p > 0.05) See also Figures S1 and S2.

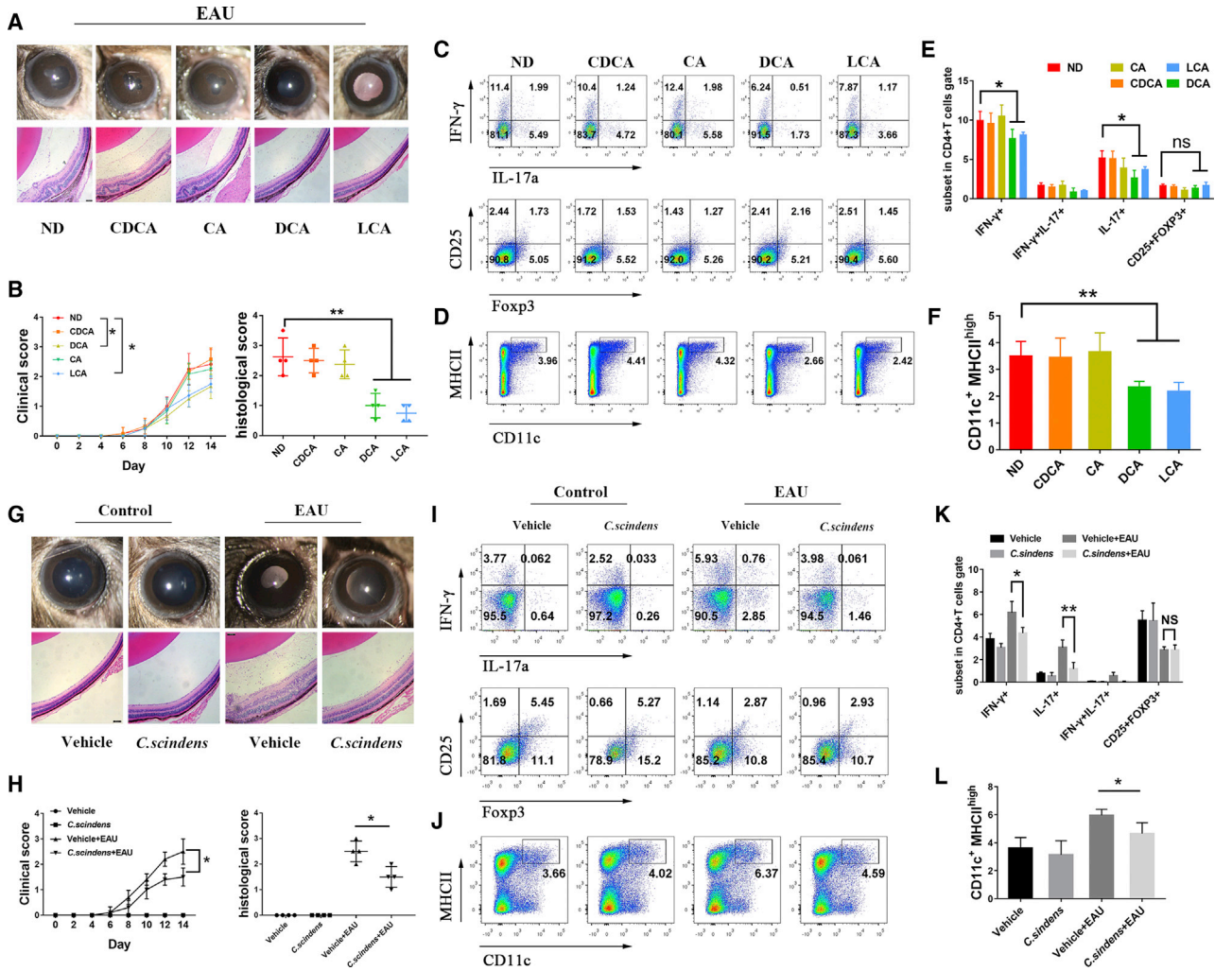

Figure 2. Secondary BA diet suppresses the severity of EAU

(A–F) C57BL/6J mice were immunized with $IRBP_{651–670}$ and CFA and fed with a CA diet, CDCA diet, DCA diet, LCA diet, and normal diet (ND) (n = 4–6 per group).

(A) Representative slit-lamp and hematoxylin and eosin (H&E) staining section images of EAU mice at the 14th day after immunization.

(B) Clinical scores were measured every 2 days after inducing EAU (the p value was evaluated at the 14th day after immunization, *$p < 0.05$), and histological scores were assessed by H&E staining of paraffin-embedded sections taken from eyes on the 14th day after immunization.

(C and E) FCM analysis of the percentage of Th1, Th17, and Treg cells in splenocytes of EAU mice.

(D and F) Flow cytometry (FCM) analysis of the percentage of $CD11c^+$MHC class II^{high} DCs in splenocytes from EAU mice.

(G–L) C57BL/6J mice were treated with antibiotics in their drinking water for 7 days and colonized with *C. scindens* by oral gavage every day for 7 days, before inducing EAU (n = 4–5 per group).

(G) Representative slit-lamp and H&E staining section images of EAU eyes at the 14th day after immunization.

(H) The clinical scores were measured every 2 days after inducing EAU (the p value was evaluated at the 14th day after immunization, *$p < 0.05$), and histological scores were assessed by H&E staining of paraffin-embedded sections at the 14th day after immunization.

(I and K) FCM analysis of the percentage of Th1, Th17, and Treg cells in splenocytes of EAU mice.

(J and L) FCM analysis of the percentage of $CD11c^+$MHC class II^{high} DCs in splenocytes of EAU mice.

Scale bars, 50 μm. Data are shown as mean ± SD. A one-way ANOVA and Kruskal-Wallis test were used. *$p < 0.05$, **$p < 0.01$; ns, not significant ($p > 0.05$). See also Figures S3–S5.

T cell differentiation, DCA-pretreated LPS-primed BMDCs were harvested and co-cultured with naive T cells isolated from EAU mice at a ratio of 1:5 (BMDCs/naive T cells). DCA was shown to decrease the development of Th1 and Th17 cells as well as the secretion of IL-17 and IFN-γ (Figures 3D–3F).

We next tested the effect of a DCA diet and *C. scindens* colonization on the expression of proinflammatory cytokines and cell surface markers in splenic DCs of EAU mice. The production of IL-1β, IL-6, TNF-α, and IL-12 by $CD11c^+$ DCs isolated from splenocytes was shown to be lower in DCA diet-treated EAU mice (Figure 3G). A similar decreased production of cytokines was observed in the *C. scindens* colonization group (Figure 3H). However, there was no difference in the expression of CD40, CD80, and CD86 in $CD11c^+$ cells (data not shown).

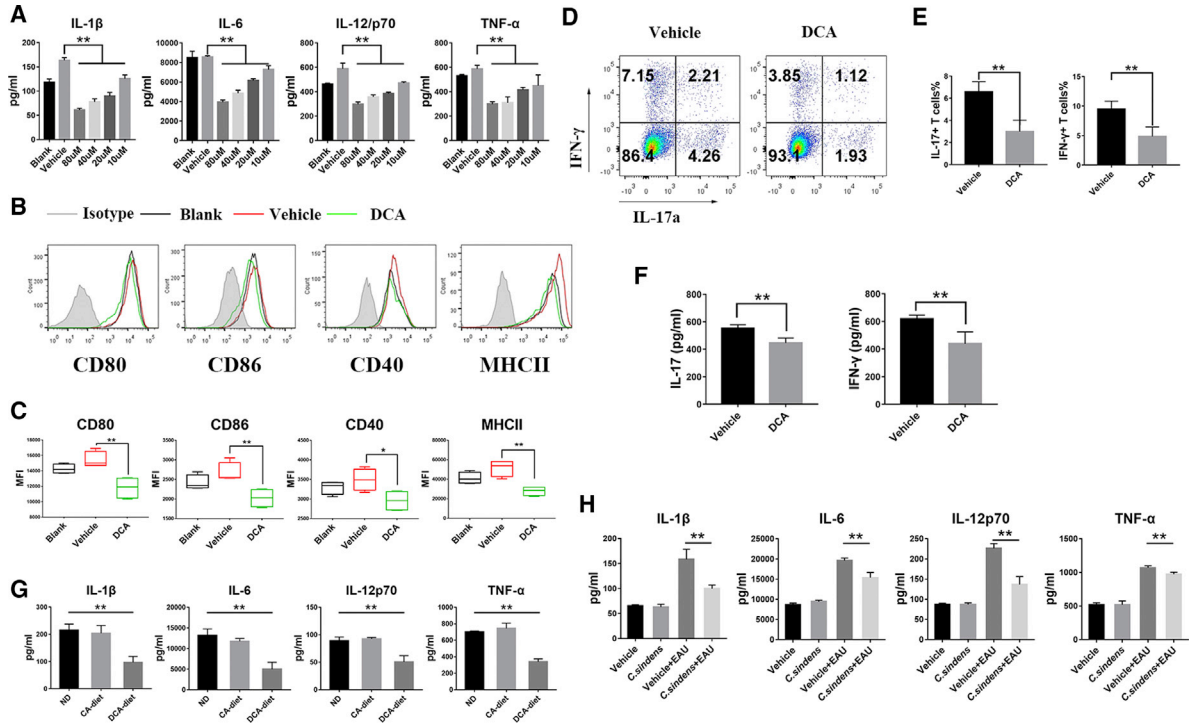

Figure 3. Secondary BA regulates the function of DCs *in vivo* and *in vitro*

(A) The expression levels of IL-1β, IL-6, IL-12p70, and TNF-α in culture supernatants of LPS-primed BMDCs treated with DCA at doses of 80, 40, 20, and 10 μM were assayed by ELISA (n = 4–6 per group).

(B and C) FCM analysis of the expression (mean fluorescence intensity [MFI]) of CD40, CD80, CD86, and MHC class II in LPS primed BMDCs treated with 80 μM DCA (n = 4 per group).

(D–F) DCA- and vehicle-treated BMDCs were co-cultured with naive T cells (BMDCs/naive T cells = 1:5, n = 4 per group). FCM analysis of the percentage of Th1 and Th17 cells (D and E). The level of IL-17 and IFN-γ in culture supernatants was tested by ELISA (F).

(G) The expression levels of IL-1β, IL-6, IL-12p70, and TNF-α in LPS-primed $CD11c^+$ cells isolated from splenocytes of C57BL/6J EAU mice treated with a DCA diet, CA diet, or ND were tested by ELISA (n = 4 per group).

(H) The expression levels of IL-1β, IL-6, IL-12p70, and TNF-α in LPS-primed $CD11c^+$ cells isolated from splenocytes of *C. scindens* colonized and control EAU mice were tested by ELISA (n = 4 per group).

Data are shown as mean ± SD. A one-way ANOVA and unpaired t test were used. *$p < 0.05$, **$p < 0.01$; ns, not significant ($p > 0.05$).

Secondary bile acid regulates DC function and suppresses the severity of EAU via TGR5 signaling

Bile acids have been shown to be able to upregulate the expression of various cell receptors in several cell types and tissues (Fiorucci et al., 2018). We tested the mRNA expression of bile acid-induced receptors, including vitamin D receptor (VDR), Takeda G protein-coupled receptor 5 (TGR5), α5β1, glucocorticoid receptor (GR), constitutive androstane receptor (CAR), farnesoid X receptor (FXR), and pregnane X receptor (PXR) in DCA-treated LPS-primed BMDCs. The expression of TGR5 mRNA was significantly increased following treatment of BMDCs with DCA (Figure S6A). A similar result was observed on the TGR5 protein level in cell lysates (Figure S6B). The recent identification of TGR5 as a bile acid-activated membrane receptor provides evidence for an anti-inflammatory function of certain bile acids (Fiorucci et al., 2018; Guo et al., 2016). We confirmed these findings by showing that INT-777, a semi-synthetic TGR5 agonist, markedly suppressed IL-1β, IL-6, IL-12p70, and TNF-α secretion and the expression of co-stimulatory molecules such as CD40, CD80, CD86, and MHC class II by LPS-primed BMDCs (Figures S6C and S6D). This effect was similar to that seen in the presence of DCA. Further experiments with $TGR5^{-/-}$ mice showed that TGR5 deficiency partially rescued the IL-1β, IL-6, IL-12p70, and TNF-α secretion and expression of co-stimulatory molecules such as CD40, CD80, CD86, and MHC class II (Figures S6E and S6F). As expected, the inhibitory effect of DCA on the antigen presentation function of BMDCs was reversed by TGR5 knockout (Figures S6G–S6I).

We subsequently investigated whether DCA suppressed the severity of EAU via TGR5 signaling. We first tested the expression of TGR5 in the retina and splenocytes of EAU mice on days 0, 7, 14, and 21 and we found that the expression of TGR5 was significantly decreased on day 14 (Figure 4A). Subsequently, $TGR5^{+/+}$ and $TGR5^{-/-}$ mice were co-housed for 7 days, and then these mice were fed with a DCA or normal diet, after which EAU was induced. TGR5 deficiency had no effect on body weight, blood glucose, and spleen weight (Figures S5H and S5I). The results showed that TGR5 knockout did not induce more serious clinical and pathological manifestations (Figures 4B and 4C), and it had no effect on Th1 and Th17 (Figures 5D and 5E), but it increased the frequency of $CD11^+$MHC class II^{high} cells (Figures 4F and

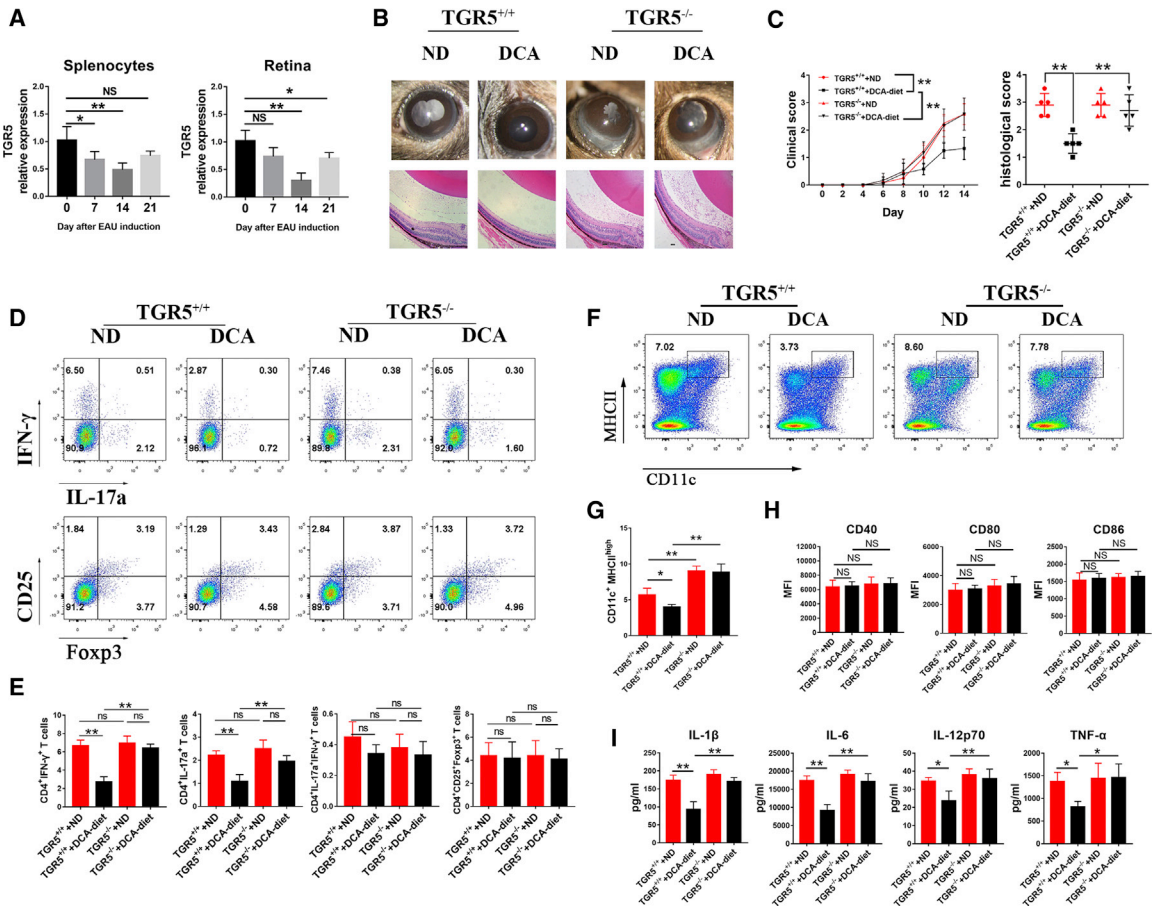

Figure 4. Secondary BA regulates DC function and suppresses the severity of EAU via TGR5 signaling

(A) The expression levels of TGR5 in the retina and splenocytes of EAU mice on days 0, 7, 14, and 21 were tested by RT-PCR (n = 4 per group).

(B–I) Co-housed TGR5$^{+/+}$ and TGR5$^{-/-}$ mice were immunized by IRBP$_{651–670}$ and CFA, and fed with an ND or DCA diet (n = 4–6 per group).

(B) Representative slit-lamp and H&E staining section images of EAU eyes at the 14th day after immunization.

(C) The clinical scores were measured every 2 days after inducing EAU (the p value was evaluated at the 14th day after immunization, **p < 0.01), and histological scores were assessed by H&E staining of paraffin-embedded sections at the 14th day after immunization.

(D and E) FCM analysis of the percentage of Th1, Th17, and Treg cells in splenocytes of EAU mice.

(F and G) FCM analysis of the percentage of CD11c^{+}MHC class II^{high} DCs in splenocytes of EAU mice.

(H) FCM analysis of the expression (MFI) of CD40, CD80, and CD86 in CD11c^{+} cells of splenocytes from EAU.

(I) The expression levels of IL-1β, IL-6, IL-12p70, and TNF-α in LPS-primed CD11c^{+} cells isolated from splenocytes of EAU were tested by ELISA.

Scale bar, 50 μm. Data are shown as mean ± SD. One-way ANOVA was used. *p < 0.05, **p < 0.01; ns, not significant (p > 0.05). See also Figure S6.

4G) in splenocytes than in TGR5$^{+/+}$ mice. However, DCA had no significant effect on IRBP$_{651–670}$-immunized TGR5$^{-/-}$ mice (Figures 4B–4G). TGR5 defiency abrogated the inhibitory effect of a DCA diet on proinflammatory cytokine production by splenic CD11c^{+} cells isolated from EAU mice (Figure 4I). No effect was however seen on cell surface marker expression (Figure 4H).

TGR5 signaling inhibits nuclear factor κB (NF-κB) activation in DCs *in vitro* and *in vivo*

The production of proinflammatory cytokines, including IL-1β, IL-6, TNF-α, and IL-12p70, in DCs is known to be mediated by the NF-κB pathway (Su et al., 2018). TGR5 activation has been shown to inhibit NF-κB activation in HepG2 cells and macrophages (Pols et al., 2011; Wang et al., 2011). In line with previous studies, we found that DCA and INT-777 significantly inhibited the phosphorylation of IκBα and nuclear p65 in LPS-primed BMDCs (Figures 5A and 5B). Furthermore, TGR5 deficiency reversed the effect of DCA and INT-777 on NF-κB pathway activation (Figure 5C). A DCA diet significantly inhibited phosphorylation of IκBα and nuclear p65 expression in splenic CD11c^{+} cells obtained from EAU mice, and TGR5 deficiency was shown to reverse this inhibition (Figure 5D).

TGR5 signaling has been shown to inhibit NF-κB activation in macrophages through IL-10 secretion induced by the cyclic AMP (cAMP) response element binding protein (CREB) (Biagioli et al., 2017; Haselow et al., 2013). However, we found that DCA reduced the production of IL-10 by LPS-primed BMDCs, and TGR5 deficiency abrogated this inhibition (Figures 5E and 5F). Additionally, DCA and TGR5 deficiency did not have an effect on CREB activation (Figure 5G).

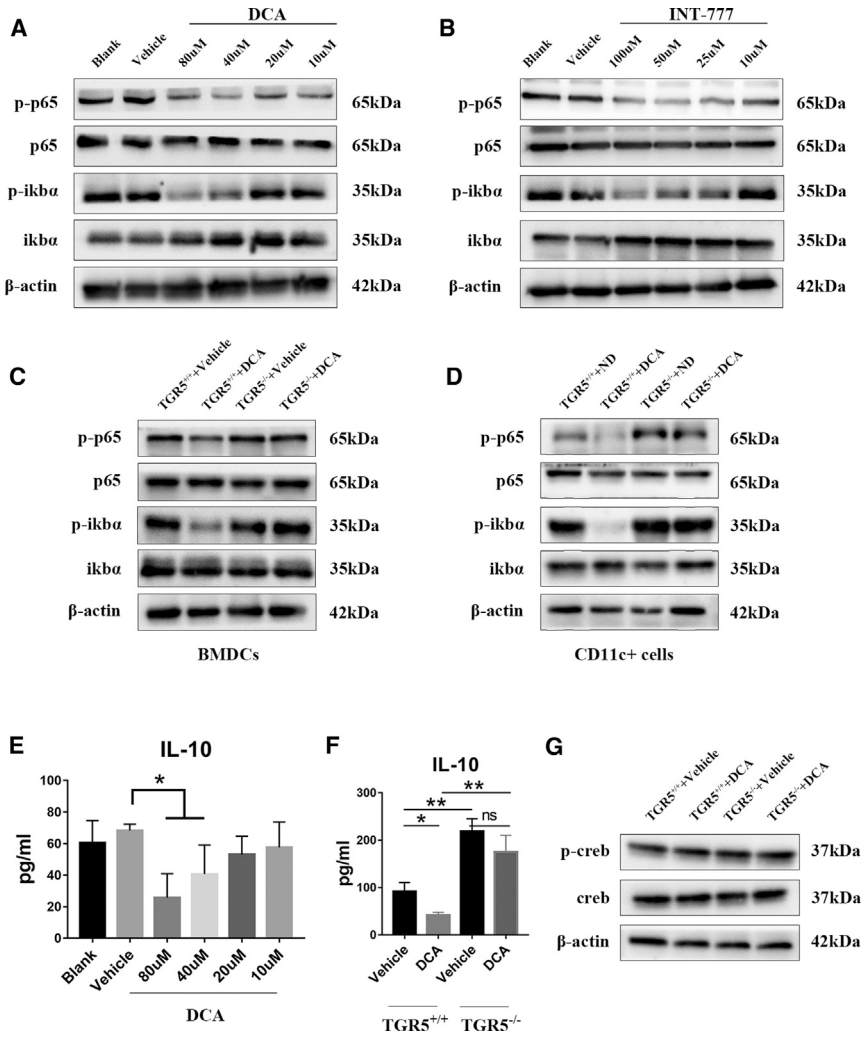

Figure 5. TGR5-mediated NF-κB inhibition is independent of IL-10 secretion

(A) The phosphorylation levels of p65 and Iκbα in LPS-primed BMDCs treated by DCA at doses of 80, 40, 20, and 10 μM were assayed by western blot.

(B) The phosphorylation levels of p65 and Iκbα in LPS-primed BMDCs treated by INT-777 at doses of 100, 50, 25, and 10 μM were assayed by western blot.

(C) The phosphorylation levels of p65 and Iκbα in LPS-primed $TGR5^{+/+}$ and $TGR5^{-/-}$ BMDCs treated by DCA or vehicle were assayed by western blot.

(D) The phosphorylation levels of p65 and Iκbα in LPS-primed $CD11c^{+}$ cells isolated from co-housed $TGR5^{+/+}$ and $TGR5^{-/-}$ EAU mice treated by a DCA diet or ND were assayed by western blot.

(E) The expression levels of IL-10 in culture supernatants of LPS-primed BMDCs treated with DCA at doses of 80, 40, 20, and 10 μM were assayed by ELISA (n = 4 per group).

(F) The expression levels of IL-10 in culture supernatants of LPS-primed $TGR5^{+/+}$ and $TGR5^{-/-}$ BMDCs treated with DCA were assayed by ELISA (n = 4 per group).

(G) The phosphorylation levels of CREB in LPS-primed $TGR5^{+/+}$ and $TGR5^{-/-}$ BMDCs treated by DCA or vehicle were assayed by western blot.

One-way ANOVA was used. Data are shown as mean ± SD. *$p < 0.05$, **$p < 0.01$; ns, not significant ($p > 0.05$).

TGR5 signaling inhibits NF-κB activation via the cAMP-PKA pathway

Agonists binding TGR5 result in the activation of adenylate cyclase, leading to an increase of cAMP, which triggers the activation of protein kinase A (PKA) (Kawamata et al., 2003). Whether the cAMP-PKA pathway is involved in TGR5-mediated NF-κB inhibition is not yet clear in DCs and was subsequently investigated in our model. DCA or INT-777 treatment increased the level of cAMP in $TGR5^{+/+}$ BMDCs, but not in $TGR5^{-/-}$ BMDCs (Figure S7A). Next, we found that forskolin (adenylate cyclase activator) or isobutylmethylxanthine (IBMX; phosphodiesterase inhibitor) reduced IL-1β, IL-6, TNF-α, and IL-12/p70 secretion in a dose-dependent manner (Figures 6A, 6B, S7B, and S7C). Furthermore, KH7 and MDL12330A (adenylate cyclase inhibitors) reversed the INT-777-mediated NF-κB inhibition (Figures 6C and 6D). Next, we investigated whether TGR5 inhibited NF-κB activation through PKA activation, which is mainly induced by intracellular cAMP. PKI (the PKA-specific inhibitory peptide) and H89 (the selective PKA inhibitor) completely blocked the INT-777-mediated NF-κB inhibition, indicating that the NF-κB inhibition induced by TGR5 signaling is PKA-dependent (Figures 6E and 6F).

DCA and TGR5 signaling inhibited activation of human monocyte-derived DCs

The results described above showed that DCA and TGR5 signaling plays an immunosuppressive effect on the development of EAU. We further tested whether DCA or TGR5 was involved in the development of human uveitis. We found that the expression of TGR5 was decreased in PBMCs from active BD patients and active VKH disease patients (Figure 7A). Additionally, we found that the expression of TGR5 was decreased in human monocyte-derived dendritic cells (Mo-DCs) from active BD patients and active VKH disease patients compared with healthy individuals (Figure 7B). Additionally, a normalized expression of TGR5 in association with the control of the intraocular inflammation was noted in BD and VKH disease patients following treatment with systemic corticosteroids and/or cyclosporine (Figures 7A and 7B). We subsequently investigated whether DCA and TGR5 signaling plays an inhibitory role in the function of human DCs. LPS-primed Mo-DCs from five active VKH disease patents and six active BD patients were incubated in the presence of DCA and INT-777 (TGR5 agonist). The results showed that DCA significantly inhibited expression of the cell surface markers CD40, CD86, and histocompatibility leukocyte antigen (HLA)-DR as well as the production of IL-1β, IL-6, TNF-α, and IL-12p70 (Figures 7C–7E). A similar result was observed in INT-777-treated Mo-DCs (Figures 7C–7E), although both

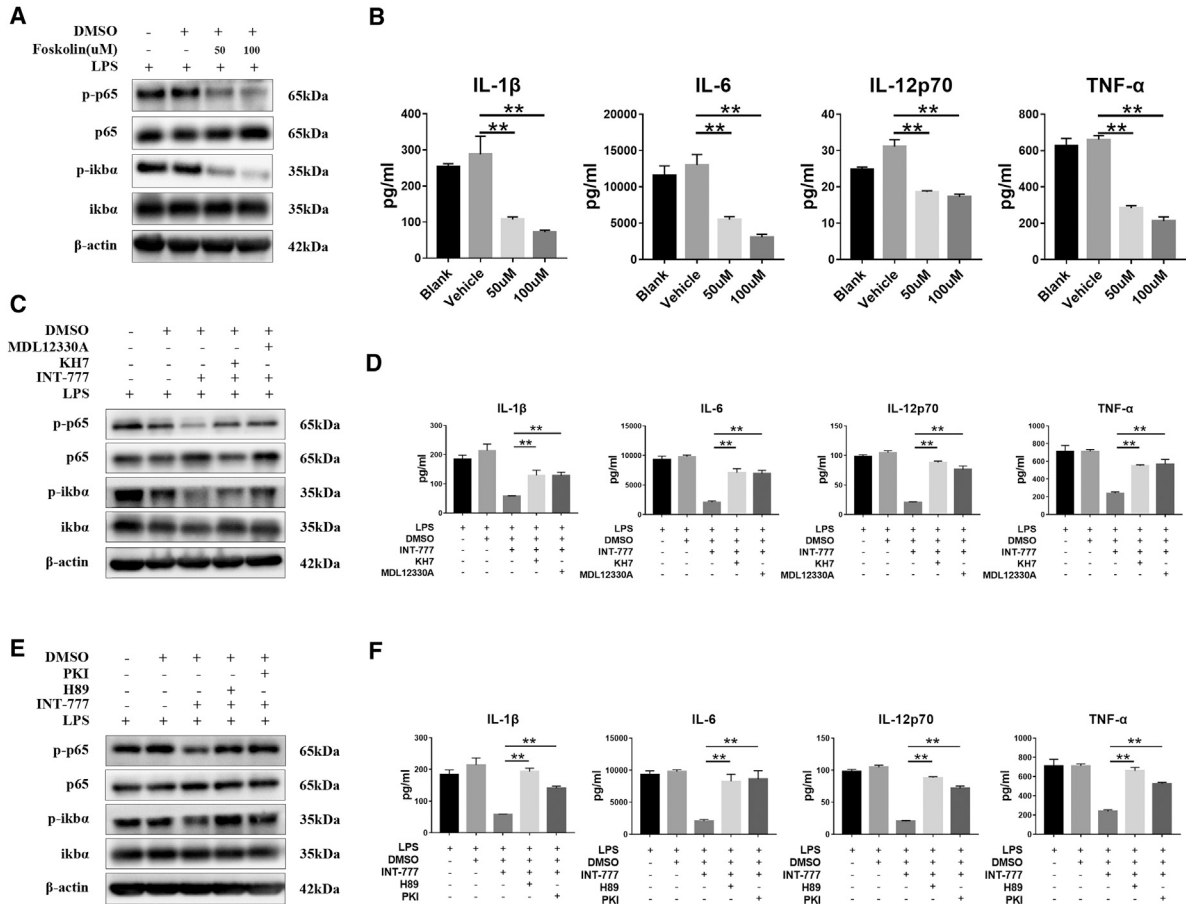

Figure 6. TGR5 signaling inhibits NF-κB activation via the cAMP-PKA pathway

(A, C, and E) The phosphorylation levels of p65 and Iκbα in LPS-primed BMDCs treated by INT-777 in the presence of forskolin (A), KH7 and MDL12300A (C), and PKI and H89 (E) were assayed by western blot.

(B, D, and F) The expression levels of IL-1β, IL-6, IL-12p70, and TNF-α in LPS-primed BMDCs treated by INT-777 in the presence of forskolin (B), KH7 and MDL12300A (D), PKI and H89 (F) were assayed by ELISA.

n = 4 per group. Data are shown as mean ± SD. A one-way ANOVA was used. *p < 0.05, **p < 0.01; ns, not significant (p > 0.05). See also Figure S7.

DCA and INT-777 had no effect on the expression of CD80 (Figure 7D). In addition, both DCA and INT-777 significantly inhibited the activation of the NF-κB pathway (Figures 7F and 7G).

DISCUSSION

In this study, we show that mice undergoing EAU have a decreasedlevel of secondary bile acids in their feces as compared to controls. Feeding mice with a diet rich in DCA (a secondary bile acid) significantly inhibited the severity of EAU, which was associated with a decreased expression of Th1 cells, Th17 cells, and CD11c^{+}MHC class II^{high} DCs. DCA inhibited NF-κB signal-mediated pro-inflammatory cytokine production by DCs through activation of the TGR5 receptor. Our further study indicated that this inhibitory effect of TGR5 was mediated through the cAMP-PKA pathway. Additionally, we showed that DCA and TGR5 agonists also inhibited activation of Mo-DCs from BD and VKH disease patients.

Gut microbiota and their metabolites have been implicated as potential modulators of the immune response in inflammatory and autoimmune diseases, including autoimmune uveitis (Huang et al., 2018a; Kalyana Chakravarthy et al., 2018; Maukonen et al., 2015; Nakamura et al., 2016; Stoll et al., 2014; Tremlett et al., 2016; Ye et al., 2018, 2020). Our current study revealed a decreased level of Ruminococcaceae and Lachnospiraceae in EAU mouse feces, the two of which have been previously identified to be decreased in various autoimmune diseases such as inflammatory bowel disease (Maukonen et al., 2015), pediatric multiple sclerosis (Tremlett et al., 2016), inflammatory uveitis (Kalyana Chakravarthy et al., 2018), enthesitis-related arthritis (Stoll et al., 2014), and type 1 diabetes (Candon et al., 2015). Ruminococcaceae and Lachnospiraceae have been reported to induce a 7α-dehydroxylation that converts the primary bile acids CA and CDCA into secondary bile acids, including DCA and LCA (Just et al., 2018; Vital et al., 2019). This observation is in agreement with a study that showed that the level of fecal secondary BAs was

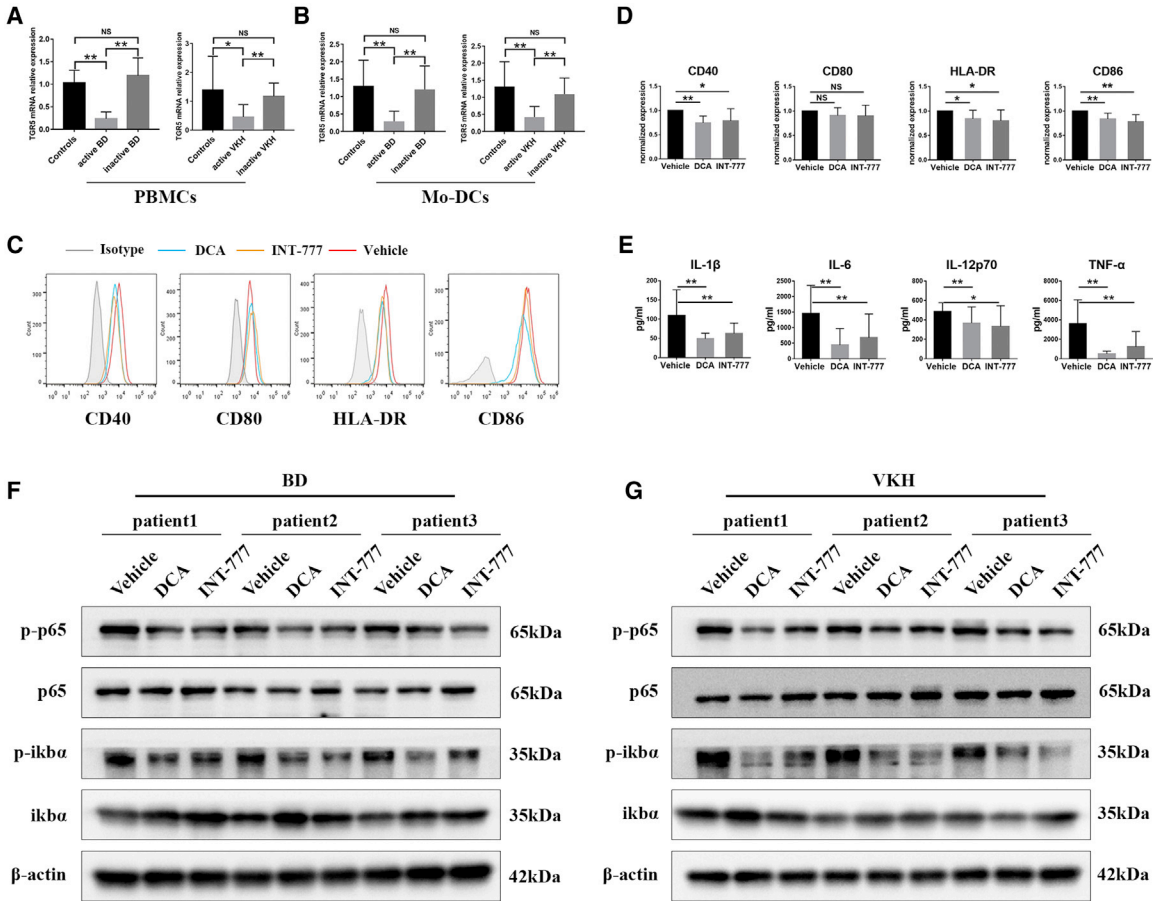

Figure 7. DCA and TGR5 signaling inhibited activation of human monocyte-derived DCs

(A) The relative mRNA expression levels of TGR5 in PBMCs of eight healthy individuals, eight active BD patients, eight inactive BD patients, eight active VKH patients, and eight inactive VKH patients were tested by RT-PCR.

(B) The relative mRNA expression levles of TGR5 in Mo-DCs of 9 healthy individuals, 12 active BD patients, 8 inactive BD patients, 8 inactive VKH patients, and 10 active VKH patients were tested by RT-PCR.

(C and D) Mo-DCs were isolated from six active BD patients and five active VKH patients, and primed by LPS. FCM analysis of the expression (MFI) of CD40, CD80, CD86, and HLA-DR in LPS-primed Mo-DCs is shown.

(E) Mo-DCs were isolated from five active BD patients and five active VKH patients, and primed by LPS. The expression levels of IL-1β, IL-6, IL-12p70, and TNF-α in cultured supernatant were tested by ELISA.

(F and G) The phosphorylation levels of p65 and Iκbα in LPS-primed Mo-DCs from BD patients (F) and VKH disease patients (G) treated by INT-777 and DCA were assayed by western blot.

Data are shown as mean ± SD. An unpaired t test, Mann-Whitney U test, paired-samples t test, and Wilcoxon test were used. *$p < 0.05$, **$p < 0.01$; ns, not significant ($p > 0.05$).

significantly lower in germ-free (GF) mice than in specific pathogen-free (SPF) mice (Song et al., 2020). In this study, we observed a decreased level of secondary bile acids in EAU mouse feces and serum. Short-chain fatty acids (SCFAs) are the main products of fermentation by saccharide microorganisms in the gut (Cummings et al., 1987). A study has indicated that fecal acetate was increased and fecal butyrate was decreased in BD patients (Consolandi et al., 2015). A lower level of butyrate-producing bacteria was also observed in the feces of BD patients (Ye et al., 2018). In the present study, we found that the concentrations of propionate and butyrate were decreased in the feces of EAU mice (Figure S8). In addition, emerging evidence has suggested that SCFAs could ameliorate the severity of endotoxin-induced uveitis and immune-mediated uveitis (Chen et al., 2017, 2021; Nakamura et al., 2017).

Bile acid dysmetabolism has also been observed in inflammatory bowel disease (IBD) patients, and it is noteworthy that only secondary bile acids (LCA and DCA) but not primary bile acids (CA and CDCA) can inhibit IL-1β and IL-18 secretion by intestinal epithelial cells (Duboc et al., 2013). Another study demonstrated that bile acids in plasma were decreased in multiple sclerosis (MS), and supplementation of the secondary bile acid TUDCA could ameliorate experimental autoimmune encephalitis (EAE) (Bhargava et al., 2020). In our study, some secondary or primary bile acids could inhibit pro-inflammatory cytokine secretion by

DCs *in vitro* (data not shown), although only secondary bile acids exhibited this inhibitory effect *in vivo*. We speculated that this may be caused by the altered gut microbiota composition in EAU mice. There are many species of bacteria in the gut that have been shown to be involved in bile acid metabolism, especially the species that belong to *Clostridium* (Fiorucci et al., 2018). Although, *Clostridium* was not found by 16S rDNA sequencing in the gut of EAU or healthy mice; however, *C. scindens* was observed to have decreased in the feces of EAU mice in this study, and it was shown to have been depleted in BD, VKH disease, and AAU patients (Huang et al., 2018a; Ye et al., 2018, 2020). *C. scindens* has been shown to successfully help rebuild a healthy bile acid metabolism in mice (Ma et al., 2018; Winkler et al., 2020). Colonization of *C. scindens* induced a rapid reduction of hepatic natural killer T (NKT) cells (Ma et al., 2018) and induced type I interferon (IFN) production in plasmacytoid DCs (Winkler et al., 2020). In line with previous studies, we show that *C. scindens* colonization restored fecal bile acid composition and suppressed the severity of EAU. These results suggest that gut microbiota-derived secondary bile acids might be key regulators in the development of autoimmune uveitis.

The anti-inflammatory effect of secondary bile acids was discovered in chronic cholestasis, where they were reported to reduce the production of IL-1β, IL-6, and TNF-α by macrophages (Calmus et al., 1992; Greve et al., 1989). Bile acids induce a polarization of macrophages toward the anti-inflammatory M2 phenotype, leading to an upregulation of IL-10 and a downregulation of the pro-inflammatory cytokines IL-6 and IFN-γ (Fiorucci et al., 2018). Besides having an influence on the innate immune response, increasing evidence suggests that secondary bile acids also play a critical role in the adaptive immune response (Bhargava et al., 2020; Hang et al., 2019). Secondary bile acids are able to reduce IL-12 production by DCs (Ichikawa et al., 2012), inhibit Th17 cell differentiation, and promote regulatory T (Treg) cell differentiation (Hang et al., 2019). Our experiment with antibiotics suggests that DCA might primarily inhibit DC activation in EAU mice.

Bile acids exhibit their anti-inflammatory effect by activating bile acid receptors, including G protein-coupled receptors (GPCRs) and nuclear receptors (Fiorucci et al., 2018). Both kinds of receptors are highly expressed on monocytes, macrophages, and DCs (Fiorucci et al., 2018). FXR and TGR5 are the two main receptors for bile acids, belonging to the nuclear receptor and GPCR, respectively (Fiorucci et al., 2018). Previous studies indicated that both FXR and TGR5 agonists effectively reverse inflammation in mouse models of vascular inflammation and EAE (Ho and Steinman, 2016; Yanguas-Casás et al., 2017). In mammals, primary bile acids (CDCA and CA) have been identified as the most potent FXR ligands, while secondary bile acids (DCA and LCA) are preferential ligands for TGR5 (Chiang, 2009). In line with this knowledge, we found that DCA induced the expression of TGR5 but had no effect on FXR.

Two studies reported that the activation of FXR by INT-747 reduced the differentiation and activation of intestinal DCs, and that progression of colitis was exacerbated in $FXR^{-/-}$ mice (Gadaleta et al., 2011; Vavassori et al., 2009). TGR5 agonists have also been reported to induce monocyte differentiation toward an IL-12 hypo-producing DC population (Ichikawa et al., 2012). However, the exact role of TGR5 signaling in DCs is not well clarified. A previous study in macrophages reported that the inhibitory effect of bile acids via TGR5 is mediated via the NF-κB pathway (Pols et al., 2011). In our study, TGR5 deficiency only partly rescued the inhibitory effect of DCA on DCs, suggesting that DCA might also exert its anti-inflammatory effect through other pathways. Further studies are needed to clarify this issue.

TGR5 and FXR have been found to modulate NLRP3 activation (Guo et al., 2016; Hao et al., 2017). In macrophages, TGR5 ligation leads to a PKA-dependent phosphorylation of NLRP3 at Ser291 (Ser295 in humans) (Guo et al., 2016). PKA kinase activation induces NLRP3 phosphorylation and promotes NLRP3 ubiquitination, thereby preventing the activation of NLRP3 inflammasomes (Guo et al., 2016). FXR also inhibits NLRP3 inflammasome activation, but it does not depend on PKA (Hao et al., 2017). PKA has also been reported to prevent the phosphorylation of Iκbα, thus inhibiting NF-κB activation (Ghosh and Baltimore, 1990; Neumann et al., 1995). We confirmed that TGR5 signaling inhibited phosphorylation of Iκbα through PKA in DCs both *in vivo* and *in vitro*. TGR5 signaling has been reported to inhibit NF-κB activation via the cAMP-PKA pathway in macrophages, and this inhibition depends on IL-10 secretion induced by CREB (Biagioli et al., 2017; Haselow et al., 2013). In our study, although we also observed that TGR5 signaling inhibited NF-κB activation, IL-10 production and phosphorylation of CREB do not seem to be involved in this process.

To verify whether our findings in animals can be extrapolated to humans, we selected two types of clinical uveitis, namely VKH disease and BD, representing an autoimmune disease and an autoinflammatory disease, respectively. In line with our previous study demonstrating decreased TGR5 expression on macrophages in active VKH disease patients (Yang et al., 2020), we herein demonstrated a decreased expression of TGR5 on DCs in both active BD and active VKH disease patients. INT-777 and DCA both inhibited pro-inflammatory cytokine and surface marker expression in Mo-DCs from BD and VKH disease patients in association with a decreased NF-κB activation. These results further supported that secondary bile acid and TGR5 play important roles in autoimmune and autoinflammatory diseases, offering potential strategies for control and treatment of these types of diseases. We have no further evidence to indicate whether gut bile acid metabolism was involved in BD or VKH disease patients, and the levels of bile acids in feces or serum of uveitis patients remain to be clarified.

In summary, we show that gut microbiota-derived secondary bile acids might be key regulators in the pathogenesis of autoimmune uveitis. Secondary bile acids were shown to inhibit NF-κB-mediated DC activation through TGR5-cAMP-PKA signaling both *in vivo* and *in vitro*. Gut microbiota and secondary bile acid composition as well as TGR5 signaling may provide potential therapeutic targets for the treatment of autoimmune and inflammatory diseases, including uveitis.

STAR★METHODS

Detailed methods are provided in the online version of this paper and include the following:

SUPPLEMENTAL INFORMATION

Supplemental information can be found online at https://doi.org/10.1016/j.celrep.2021.109726.

ACKNOWLEDGMENTS

The authors thank Prof. Peizeng Yang of Chongqing Key Laboratory of Ophthalmology for expert advice on this study. The authors also thank the Shanghai Applied Protein Technology Co., Ltd for 16S rDNA sequencing. This work was supported by the National Natural Science Foundation Project of China (81770913, 81974131, 81900887, 81800813, and 82000884).

AUTHOR CONTRIBUTIONS

J.H. and H.L. designed the experiments, interpreted the data, and wrote the manuscript. J.H., S.Y., S.P., G.Y., X.Y., and X.H. performed experiments. J.H., C.W., Y.Z., and Q.C. interpreted the data. J.H. and H.L. edited the manuscript.

DECLARATION OF INTERESTS

The authors declare no competing interests.

Received: September 6, 2020
Revised: August 10, 2021
Accepted: August 24, 2021
Published: September 21, 2021

REFERENCES

Abdollahi-Roodsaz, S., Abramson, S.B., and Scher, J.U. (2016). The metabolic role of the gut microbiota in health and rheumatic disease: Mechanisms and interventions. Nat. Rev. Rheumatol. *12*, 446–455.

Agarwal, R.K., Silver, P.B., and Caspi, R.R. (2012). Rodent models of experimental autoimmune uveitis. Methods Mol. Biol. *900*, 443–469.

Allenspach, E.J., Lemos, M.P., Porrett, P.M., Turka, L.A., and Laufer, T.M. (2008). Migratory and lymphoid-resident dendritic cells cooperate to efficiently prime naive CD4 T cells. Immunity *29*, 795–806.

Bhargava, P., Smith, M.D., Mische, L., Harrington, E., Fitzgerald, K.C., Martin, K., Kim, S., Reyes, A.A., Gonzalez-Cardona, J., Volsko, C., et al. (2020). Bile acid metabolism is altered in multiple sclerosis and supplementation ameliorates neuroinflammation. J. Clin. Invest. *130*, 3467–3482.

Biagioli, M., Carino, A., Cipriani, S., Francisci, D., Marchianò, S., Scarpelli, P., Sorcini, D., Zampella, A., and Fiorucci, S. (2017). The bile acid receptor GPBAR1 regulates the M1/M2 phenotype of intestinal macrophages and activation of GPBAR1 rescues mice from murine colitis. J. Immunol. *199*, 718–733.

Calmus, Y., Guechot, J., Podevin, P., Bonnefis, M.T., Giboudeau, J., and Poupon, R. (1992). Differential effects of chenodeoxycholic and ursodeoxycholic acids on interleukin 1, interleukin 6 and tumor necrosis factor-α production by monocytes. Hepatology *16*, 719–723.

Candon, S., Perez-Arroyo, A., Marquet, C., Valette, F., Foray, A.P., Pelletier, B., Milani, C., Ventura, M., Bach, J.F., and Chatenoud, L. (2015). Antibiotics in early life alter the gut microbiome and increase disease incidence in a spontaneous mouse model of autoimmune insulin-dependent diabetes. PLoS ONE *10*, e0125448.

Caporaso, J.G., Kuczynski, J., Stombaugh, J., Bittinger, K., Bushman, F.D., Costello, E.K., Fierer, N., Peña, A.G., Goodrich, J.K., Gordon, J.I., et al. (2010). QIIME allows analysis of high-throughput community sequencing data. Nat. Methods *7*, 335–336.

Chen, X., Su, W., Wan, T., Yu, J., Zhu, W., Tang, F., Liu, G., Olsen, N., Liang, D., and Zheng, S.G. (2017). Sodium butyrate regulates Th17/Treg cell balance to ameliorate uveitis via the Nrf2/HO-1 pathway. Biochem. Pharmacol. *142*, 111–119.

Chen, N., Wu, J., Wang, J., Piri, N., Chen, F., Xiao, T., Zhao, Y., Sun, D., Kaplan, H.J., and Shao, H. (2021). Short chain fatty acids inhibit endotoxin-induced uveitis and inflammatory responses of retinal astrocytes. Exp. Eye Res. *206*, 108520.

Chiang, J.Y. (2009). Bile acids: Regulation of synthesis. J. Lipid Res. *50*, 1955–1966.

Consolandi, C., Turroni, S., Emmi, G., Severgnini, M., Fiori, J., Peano, C., Biagi, E., Grassi, A., Rampelli, S., Silvestri, E., et al. (2015). Behçet's syndrome patients exhibit specific microbiome signature. Autoimmun. Rev. *14*, 269–276.

Cummings, J.H., Pomare, E.W., Branch, W.J., Naylor, C.P., and Macfarlane, G.T. (1987). Short chain fatty acids in human large intestine, portal, hepatic and venous blood. Gut *28*, 1221–1227.

Dapito, D.H., Mencin, A., Gwak, G.Y., Pradere, J.P., Jang, M.K., Mederacke, I., Caviglia, J.M., Khiabanian, H., Adeyemi, A., Bataller, R., et al. (2012). Promotion of hepatocellular carcinoma by the intestinal microbiota and TLR4. Cancer Cell *21*, 504–516.

Dart, A. (2018). Gut microbiota bile acid metabolism controls cancer immunosurveillance. Nat. Rev. Microbiol. *16*, 453.

Duboc, H., Rajca, S., Rainteau, D., Benarous, D., Maubert, M.A., Quervain, E., Thomas, G., Barbu, V., Humbert, L., Despras, G., et al. (2013). Connecting dysbiosis, bile-acid dysmetabolism and gut inflammation in inflammatory bowel diseases. Gut *62*, 531–539.

Fiorucci, S., Biagioli, M., Zampella, A., and Distrutti, E. (2018). Bile acids activated receptors regulate innate immunity. Front. Immunol. *9*, 1853.

Gadaleta, R.M., van Erpecum, K.J., Oldenburg, B., Willemsen, E.C., Renooij, W., Murzilli, S., Klomp, L.W., Siersema, P.D., Schipper, M.E., Danese, S., et al. (2011). Farnesoid X receptor activation inhibits inflammation and preserves the intestinal barrier in inflammatory bowel disease. Gut *60*, 463–472.

Ghosh, S., and Baltimore, D. (1990). Activation in vitro of NF-κB by phosphorylation of its inhibitor IκB. Nature *344*, 678–682.

Greve, J.W., Gouma, D.J., and Buurman, W.A. (1989). Bile acids inhibit endotoxin-induced release of tumor necrosis factor by monocytes: An in vitro study. Hepatology *10*, 454–458.

Guo, C., Xie, S., Chi, Z., Zhang, J., Liu, Y., Zhang, L., Zheng, M., Zhang, X., Xia, D., Ke, Y., et al. (2016). Bile acids control inflammation and metabolic disorder through inhibition of NLRP3 inflammasome. Immunity *45*, 944.

Hang, S., Paik, D., Yao, L., Kim, E., Trinath, J., Lu, J., Ha, S., Nelson, B.N., Kelly, S.P., Wu, L., et al. (2019). Bile acid metabolites control T_H17 and T_{reg} cell differentiation. Nature *576*, 143–148.

Hao, H., Cao, L., Jiang, C., Che, Y., Zhang, S., Takahashi, S., Wang, G., and Gonzalez, F.J. (2017). Farnesoid X receptor regulation of the NLRP3 inflammasome underlies cholestasis-associated sepsis. Cell Metab. *25*, 856–867.e5.

Haselow, K., Bode, J.G., Wammers, M., Ehlting, C., Keitel, V., Kleinebrecht, L., Schupp, A.K., Häussinger, D., and Graf, D. (2013). Bile acids PKA-dependently induce a switch of the IL-10/IL-12 ratio and reduce proinflammatory capability of human macrophages. J. Leukoc. Biol. *94*, 1253–1264.

Ho, P.P., and Steinman, L. (2016). Obeticholic acid, a synthetic bile acid agonist of the farnesoid X receptor, attenuates experimental autoimmune encephalomyelitis. Proc. Natl. Acad. Sci. USA *113*, 1600–1605.

Huang, X., Ye, Z., Cao, Q., Su, G., Wang, Q., Deng, J., Zhou, C., Kijlstra, A., and Yang, P. (2018a). Gut microbiota composition and fecal metabolic phenotype in patients with acute anterior uveitis. Invest. Ophthalmol. Vis. Sci. *59*, 1523–1531.

Huang, Y., He, J., Liang, H., Hu, K., Jiang, S., Yang, L., Mei, S., Zhu, X., Yu, J., Kijlstra, A., et al. (2018b). Aryl hydrocarbon receptor regulates apoptosis and inflammation in a murine model of experimental autoimmune uveitis. Front. Immunol. *9*, 1713.

Ichikawa, R., Takayama, T., Yoneno, K., Kamada, N., Kitazume, M.T., Higuchi, H., Matsuoka, K., Watanabe, M., Itoh, H., Kanai, T., et al. (2012). Bile acids induce monocyte differentiation toward interleukin-12 hypo-producing dendritic cells via a TGR5-dependent pathway. Immunology *136*, 153–162.

International Study Group for Behçet's Disease (1990). Criteria for diagnosis of Behçet's disease. Lancet *335*, 1078–1080.

Janowitz, C., Nakamura, Y.K., Metea, C., Gligor, A., Yu, W., Karstens, L., Rosenbaum, J.T., Asquith, M., and Lin, P. (2019). Disruption of intestinal homeostasis and intestinal microbiota during experimental autoimmune uveitis. Invest. Ophthalmol. Vis. Sci. *60*, 420–429.

Jia, W., Xie, G., and Jia, W. (2018). Bile acid-microbiota crosstalk in gastrointestinal inflammation and carcinogenesis. Nat. Rev. Gastroenterol. Hepatol. *15*, 111–128.

Just, S., Mondot, S., Ecker, J., Wegner, K., Rath, E., Gau, L., Streidl, T., Hery-Arnaud, G., Schmidt, S., Lesker, T.R., et al. (2018). The gut microbiota drives the impact of bile acids and fat source in diet on mouse metabolism. Microbiome *6*, 134.

Kalyana Chakravarthy, S., Jayasudha, R., Sai Prashanthi, G., Ali, M.H., Sharma, S., Tyagi, M., and Shivaji, S. (2018). Dysbiosis in the gut bacterial microbiome of patients with uveitis, an inflammatory disease of the eye. Indian J. Microbiol. *58*, 457–469.

Kawamata, Y., Fujii, R., Hosoya, M., Harada, M., Yoshida, H., Miwa, M., Fukusumi, S., Habata, Y., Itoh, T., Shintani, Y., et al. (2003). A G protein-coupled receptor responsive to bile acids. J. Biol. Chem. *278*, 9435–9440.

Lutz, M.B., Kukutsch, N., Ogilvie, A.L., Rössner, S., Koch, F., Romani, N., and Schuler, G. (1999). An advanced culture method for generating large quantities of highly pure dendritic cells from mouse bone marrow. J. Immunol. Methods *223*, 77–92.

Ma, C., Han, M., Heinrich, B., Fu, Q., Zhang, Q., Sandhu, M., Agdashian, D., Terabe, M., Berzofsky, J.A., Fako, V., et al. (2018). Gut microbiome-mediated bile acid metabolism regulates liver cancer via NKT cells. Science *360*, eaan5931.

Maukonen, J., Kolho, K.L., Paasela, M., Honkanen, J., Klemetti, P., Vaarala, O., and Saarela, M. (2015). Altered fecal microbiota in paediatric inflammatory bowel disease. J. Crohn's Colitis *9*, 1088–1095.

Miserocchi, E., Fogliato, G., Modorati, G., and Bandello, F. (2013). Review on the worldwide epidemiology of uveitis. Eur. J. Ophthalmol. *23*, 705–717.

Mooranian, A., Zamani, N., Takechi, R., Al-Sallami, H., Mikov, M., Goločorbin-Kon, S., Kovacevic, B., Arfuso, F., and Al-Salami, H. (2018). Pharmacological effects of nanoencapsulation of human-based dosing of probucol on ratio of secondary to primary bile acids in gut, during induction and progression of type 1 diabetes. Artif. Cells Nanomed. Biotechnol. *46* (*Suppl 3*), S748–S754.

Nakamura, Y.K., Metea, C., Karstens, L., Asquith, M., Gruner, H., Moscibrocki, C., Lee, I., Brislawn, C.J., Jansson, J.K., Rosenbaum, J.T., and Lin, P. (2016). Gut microbial alterations associated with protection from autoimmune uveitis. Invest. Ophthalmol. Vis. Sci. *57*, 3747–3758.

Nakamura, Y.K., Janowitz, C., Metea, C., Asquith, M., Karstens, L., Rosenbaum, J.T., and Lin, P. (2017). Short chain fatty acids ameliorate immune-mediated uveitis partially by altering migration of lymphocytes from the intestine. Sci. Rep. *7*, 11745.

Neumann, M., Grieshammer, T., Chuvpilo, S., Kneitz, B., Lohoff, M., Schimpl, A., Franza, B.R., Jr., and Serfling, E. (1995). RelA/p65 is a molecular target for the immunosuppressive action of protein kinase A. EMBO J. *14*, 1991–2004.

Pols, T.W., Nomura, M., Harach, T., Lo Sasso, G., Oosterveer, M.H., Thomas, C., Rizzo, G., Gioiello, A., Adorini, L., Pellicciari, R., et al. (2011). TGR5 activation inhibits atherosclerosis by reducing macrophage inflammation and lipid loading. Cell Metab. *14*, 747–757.

Read, R.W., Holland, G.N., Rao, N.A., Tabbara, K.F., Ohno, S., Arellanes-Garcia, L., Pivetti-Pezzi, P., Tessler, H.H., and Usui, M. (2001). Revised diagnostic criteria for Vogt-Koyanagi-Harada disease: Report of an international committee on nomenclature. Am. J. Ophthalmol. *131*, 647–652.

Shapiro, H., Kolodziejczyk, A.A., Halstuch, D., and Elinav, E. (2018). Bile acids in glucose metabolism in health and disease. J. Exp. Med. *215*, 383–396.

Song, X., Sun, X., Oh, S.F., Wu, M., Zhang, Y., Zheng, W., Geva-Zatorsky, N., Jupp, R., Mathis, D., Benoist, C., and Kasper, D.L. (2020). Microbial bile acid metabolites modulate gut $ROR\gamma^+$ regulatory T cell homeostasis. Nature *577*, 410–415.

Stoll, M.L., Kumar, R., Morrow, C.D., Lefkowitz, E.J., Cui, X., Genin, A., Cron, R.Q., and Elson, C.O. (2014). Altered microbiota associated with abnormal humoral immune responses to commensal organisms in enthesitis-related arthritis. Arthritis Res. Ther. *16*, 486.

Su, H., Zhang, Z., Liu, Z., Peng, B., Kong, C., Wang, H., Zhang, Z., and Xu, Y. (2018). *Mycobacterium tuberculosis* PPE60 antigen drives Th1/Th17 responses via Toll-like receptor 2-dependent maturation of dendritic cells. J. Biol. Chem. *293*, 10287–10302.

Taylor, S.A., and Green, R.M. (2018). Bile acids, microbiota, and metabolism. Hepatology *68*, 1229–1231.

Tremlett, H., Fadrosh, D.W., Faruqi, A.A., Zhu, F., Hart, J., Roalstad, S., Graves, J., Lynch, S., and Waubant, E.; US Network of Pediatric MS Centers (2016). Gut microbiota in early pediatric multiple sclerosis: A case-control study. Eur. J. Neurol. *23*, 1308–1321.

Vavassori, P., Mencarelli, A., Renga, B., Distrutti, E., and Fiorucci, S. (2009). The bile acid receptor FXR is a modulator of intestinal innate immunity. J. Immunol. *183*, 6251–6261.

Vital, M., Rud, T., Rath, S., Pieper, D.H., and Schlüter, D. (2019). Diversity of bacteria exhibiting bile acid-inducible 7α-dehydroxylation genes in the human gut. Comput. Struct. Biotechnol. J. *17*, 1016–1019.

Wang, Y.D., Chen, W.D., Yu, D., Forman, B.M., and Huang, W. (2011). The G-protein-coupled bile acid receptor, Gpbar1 (TGR5), negatively regulates hepatic inflammatory response through antagonizing nuclear factor κ light-chain enhancer of activated B cells (NF-κB) in mice. Hepatology *54*, 1421–1432.

Winkler, E.S., Shrihari, S., Hykes, B.L., Jr., Handley, S.A., Andhey, P.S., Huang, Y.S., Swain, A., Droit, L., Chebrolu, K.K., Mack, M., et al. (2020). The Intestinal Microbiome Restricts Alphavirus Infection and Dissemination through a Bile Acid-Type I IFN Signaling Axis. Cell *182*, 901–918.e18.

Wu, W.H., Zegarra-Ruiz, D.F., and Diehl, G.E. (2020). Intestinal microbes in autoimmune and inflammatory disease. Front. Immunol. *11*, 597966.

Yang, P., Zhong, Y., Du, L., Chi, W., Chen, L., Zhang, R., Zhang, M., Wang, H., Lu, H., Yang, L., et al. (2018). Development and evaluation of diagnostic criteria for Vogt-Koyanagi-Harada disease. JAMA Ophthalmol. *136*, 1025–1031.

Yang, J., Hu, J., Feng, L., Yi, S., Ye, Z., Lin, M., Liu, X., Pu, Y., Kijlstra, A., Yang, P., and Li, H. (2020). Decreased expression of TGR5 in Vogt-Koyanagi-Harada (VKH) disease. Ocul. Immunol. Inflamm. *28*, 200–208.

Yanguas-Casás, N., Barreda-Manso, M.A., Nieto-Sampedro, M., and Romero-Ramírez, L. (2017). TUDCA: An agonist of the bile acid receptor GPBAR1/TGR5 with anti-inflammatory effects in microglial cells. J. Cell. Physiol. *232*, 2231–2245.

Ye, Z., Zhang, N., Wu, C., Zhang, X., Wang, Q., Huang, X., Du, L., Cao, Q., Tang, J., Zhou, C., et al. (2018). A metagenomic study of the gut microbiome in Behcet's disease. Microbiome *6*, 135.

Ye, Z., Wu, C., Zhang, N., Du, L., Cao, Q., Huang, X., Tang, J., Wang, Q., Li, F., Zhou, C., et al. (2020). Altered gut microbiome composition in patients with Vogt-Koyanagi-Harada disease. Gut Microbes *11*, 539–555.

STAR★METHODS

KEY RESOURCES TABLE

REAGENT or RESOURCE	SOURCE	IDENTIFIER
Antibodies		
Anti-mouse CD4 APC	eBioscience	Cat# 17-0042-81; RRID:AB_469322
Anti-mouse IL-17a PE	eBioscience	Cat# 12-7177-81; RRID:AB_763582
Anti-mouse IFN-γ PE-cy7	eBioscience	Cat# 25-7311-82; RRID:AB_469680
Anti-mouse CD25 PE	eBioscience	Cat# 12-0251-81; RRID:AB_465606
Anti-mouse Foxp3 PE-cy7	eBioscience	Cat# 25-5773-80; RRID:AB_891554
Anti-mouse CD11c APC	BioLegend	Cat# 117310; RRID:AB_313779
Anti-mouse CD40 FITC	BioLegend	Cat# 124607; RRID:AB_1134090
Anti-mouse MHCII PE	eBioscience	Cat# 12-5321-81; RRID:AB_465927
Anti-mouse CD80 PE	eBioscience	Cat# 12-0801-81; RRID:AB_465751
Anti-mouse CD86 FITC	eBioscience	Cat# 11-0860-82; RRID:AB_465145
Anti-human CD80 PE	BioLegend	Cat# 375410; RRID:AB_2890820
Anti-human CD86 PE-cy7	BioLegend	Cat# 374209; RRID:AB_2728391
Anti-human HLA-DR PE-cy5.5	BioLegend	Cat# 307629; RRID:AB_893575
Anti-human CD40 FITC	BioLegend	Cat# 334305; RRID:AB_1186056
Mouse CD4 microbeads	Miltenyi Biotec	Cat# 130-049-201; RRID:AB_2722753
Human CD14 microbeads	Miltenyi Biotec	Cat# 130-097-052; RRID:AB_2665482
Anti-TGR5	Abcam	Cat# ab72608; RRID:AB_2112165
Anti-P65	Abcam	Cat# ab16502; RRID:AB_443394
Anti-NF-κB p65 (Phospho Ser536)	CST	Cat# 3033T; RRID:AB_331284
Anti-Ikbα	Abcam	Cat# ab32518; RRID:AB_733068
Anti-Ikbα (phospho S36)	Abcam	Cat# ab133462; RRID:AB_2801653
Anti-CREB	Abcam	Cat# ab32515; RRID:AB_2292301
Anti-CREB(phosphor S133)	Abcam	Cat# ab32096; RRID:AB_731734
Anti-β-actin	Abcam	Cat# ab8227; RRID:AB_2305186
Experimental models: Organisms/strains		
C57BL/6j mice	Jachson Lab	N/A
$TGR5^{-/-}$ mice	Viewsolid biotech	N/A
Bacterial and virus strains		
Clostridium scindens	ATCC	ATCC35704
Chemicals, peptides, and recombinant proteins		
$IRBP_{651-670}$	Sangon Biotech	N/A
Mycobacterium tuberculosis strain H37Ra	BD	Cat# 231141
Bordetella pertussis toxin	Sigma	Cat# P7208
CFA	Sigma	Cat# F5881
QIAamp Fast DNA Stool Mini Kit	QIAGEN	Cat# 51604
Neomycin	Sigma	Cat# N6386
Ampicillin	Sigma	Cat# A5354
Metronidazole	Sigma	Cat# 16677
Vancomycin	Sigma	Cat# V2002
TRIzol Reagent	Invitrogen	Cat# 15596026
PrimeScript RT reagent Kit	Takara	Cat# DRR047A
iTaq Universal SYBR Green Supermix	BIO-RAD	Cat# 1725124

(*Continued on next page*)

Continued

REAGENT or RESOURCE	SOURCE	IDENTIFIER
mouse GM-CSF	R&D	Cat# 415-ML-50
mouse IL-4	R&D	Cat# 404-ML-50
Lipopolysaccharide	Sigma	Cat# L2880
DCA	Sigma	Cat# L6250
INT-777	MedChemExpress	Cat# HY-15677
Forskolin	MedChemExpress	Cat# HY-15371
IBMX	MedChemExpress	Cat# HY-12318
KH7	MedChemExpress	Cat# HY-103194
MDL12330A	Sigma	Cat# 444200
PKI	MedChemExpress	Cat# HY-P0222
H89	MedChemExpress	Cat# HY-15979
Foxp3 / Transcription Factor Staining Buffer Set Kit	Invitrogen	Cat# 00-5523-00
PMA	Sigma	Cat# P1585
Ionomycin	Sigma	Cat# I3909
brefeldin A	Sigma	Cat# B6542
human GM-CSF	AcroBiosystems	Cat# GMF-H8214
human GM-IL-4	AcroBiosystems	Cat# IL-4-H4218
Mouse TNF-α DuoSet ELISA	R&D	Cat# DY410-05
Mouse IL-6 DouSet ELISA	R&D	Cat# DY406-05
Mouse IL-1β DouSet ELISA	R&D	Cat# DY401-05
Mouse IL-17 DouSet ELISA	R&D	Cat# DY421-05
Mouse IFN-γ DouSet ELISA	R&D	Cat# DY485-05
Mouse IL-10 DouSet ELISA	R&D	Cat# DY-417-05
Mouse IL-12/P70 DouSet ELISA	R&D	Cat# DY-419-05
Mouse IL-23 DouSet ELISA	R&D	Cat# DY1887-05
Human IL-1β DouSet ELISA	R&D	Cat# DY201
Human IL-6 DouSet ELISA	R&D	Cat# DY206
Human IL-12/P70 ELISA KIT	Invitrogen	Cat# BMS238
Human TNF-α DouSet ELISA	R&D	Cat# DY210
Deposited data		
Microbiota 16S rRNA gene sequences (NCBI GenBank)	This paper	PRJNA718486
Oligonucleotides		
Mouse PXR F: 5′-GACCTGCCTATTG AGGACCA-3′	Sangon Biotech	N/A
Mouse PXR R: 5′-TTCTGGAAGCCACCATTAGG-3′	Sangon Biotech	N/A
Mouse α5β1 F: 5′-AGCGACTGGAATCC TCAAGA-3′	Sangon Biotech	N/A
Mouse α5β1 R: 5′-TGCTGAGTCCTGT CACCTTG-3′	Sangon Biotech	N/A
Mouse GR F: 5′-AGGCCGCTCAGTGTTTTCTA-3′	Sangon Biotech	N/A
Mouse GR R: 5′-TACAGCTTCCACACGTCAGC-3′	Sangon Biotech	N/A
Mouse TGR5 F: 5′-TTCTCTCTGTCCG CGTGTTG-3′	Sangon Biotech	N/A
Mouse TGR5 R: 5′-GGTGCTGCCCAA TGAGATGA-3′	Sangon Biotech	N/A
Mouse VDR F: 5′-GATGAGGAGGTGC AGCGTAA-3′	Sangon Biotech	N/A

(*Continued on next page*)

Continued

REAGENT or RESOURCE	SOURCE	IDENTIFIER
Mouse VDR R: 5′-GTCGTAGGTCT TGTGGTGGG-3′	Sangon Biotech	N/A
Mouse FXR F: 5′-AGGGGATGAGC TGTGTGTTG –3′	Sangon Biotech	N/A
Mouse FXR R: 5′-ACACTGGATTTCAGTT AACAAACCT-3′	Sangon Biotech	N/A
Mouse CAR F: 5′-GGAGGACCAGA TCTCCCTTC-3′	Sangon Biotech	N/A
Mouse CAR R: 5′-CTCGTACTGGA ACCCTGCAT-3′	Sangon Biotech	N/A
Mouse GAPDH F: 5′-ACCCAGAA GACTGTGGATGG-3′	Sangon Biotech	N/A
Mouse GAPDH R: 5′-CACATTGGG GGTAGGAACAC-3′	Sangon Biotech	N/A
Software and algorithms		
GraphPad Prism version 7.0	GraphPad Software	https://www.graphpad.com
UPARSE	PMID: 23955772	http://www.drive5.com/usearch/
QIIME software	PMID: 20383131	http://qiime.org/
SPSS version 22.0	SPSS	https://www.ibm.com/products/spss-statistics
Flowjo version 10.0	Tree	https://www.flowjo.com/

RESOURCE AVAILABILITY

Lead contact

Further information and requests for resources and reagents should be directed to and will be fulfilled by the Lead Contact, Hong Li (lihongcqmu@163.com).

Materials availability

This study did not generate new unique reagents.

Data and code availability

16 s rDNA sequencing data for all samples have been deposited in NCBI and are publicly available as of the date of publication. Accession numbers are listed in the Key resources table. Original western blot images and microscopy data reported in this paper will be shared by the lead contact upon request.

This study did not generate any unique code.

Any additional information required to reanalyze the data reported in this paper is available from the lead contact upon request.

EXPERIMENTAL MODEL AND SUBJECT DETAILS

Mice

SPF C57BL/6J (TGR5$^{+/+}$) mice were purchased from Jackson laboratory (Bar Harbor, ME). TGR5$^{-/-}$ mice (C57BL/6J background) were purchased from Viewsolid biotech (Beijing, China). 6- to 8-week-old age-matched female mice were used (4-6 mice per group). Animal protocols were approved by the Animal Care and Use Committee of our hospital. The study conformed to the ARVO statement for the Use of Animals in Ophthalmic and Vision Research.

Human study

Active BD patients (n = 22), active VKH patients (n = 21), inactive BD patients (n = 8), inactive VKH patients (n = 8) and healthy donors (n = 16) were enrolled in our hospital and gave written informed consent for this study. All enrolled active BD patients were diagnosed according to the international nomenclature committee (International Study Group for Behçet's Disease, 1990), and all active VKH patients were diagnosed according to the international and Chinese nomenclature committee (Read et al., 2001; Yang et al.,

2018). All patients came to our hospital for the first time and did not receive treatment or had stopped taking medicine for at least one week prior to blood collection. All procedures strictly followed the principles of the Helsinki Declaration and were approved by the ethics committee of our hospital.

METHOD DETAILS

Induction of EAU

EAU was induced in C57BL/6J mice and TGR5$^{-/-}$ mice by subcutaneous injection of 300 μg human IRBP peptide amino acid residues 651–670 (IRBP$_{651-670}$) in 0.2 mL emulsion 1:1 (vol/vol) with complete freund's adjuvant containing *Mycobacterium tuberculosis* strain H37Ra (2.5 mg/mL, BD Biosciences, USA). At the time of immunization, mice also received an intraperitoneal injection with *Bordetella pertussis* toxin (PTX, 0.5 μg per mouse). These mice received another injection with PTX after 2 days. This high IRBP EAU protocol has been shown earlier to induce a very severe EAU (Huang et al., 2018b). In separate experiments, mice were given a specific bile acids-diet (0.02% CDCA, 0.02% CA, 0.02% DCA and 0.01% LCA) after inducing EAU or received *C. scindens* (ATCC35704, MD, USA) orally before inducing EAU (details are shown below). Clinical uveitis was scored by the investigator in a blinded fashion (blinded to genotype and treatment groups) by slit lamp.

Fecal sample collection and DNA extraction

Fecal samples were collected from C57BL/6J mice on day 14 after IRBP$_{651-670}$ immunization. Fecal samples from C57BL/6J mice receiving incomplete freund's adjuvant were served as controls. Total genomic DNA from fecal samples was extracted using the QIAamp Fast DNA Stool Mini Kit (QIAGEN, Hilden, Germany) according to the manufacturer's instructions. DNA concentration and purity was monitored on 1% agarose gels.

16S rDNA sequencing

Fecal DNA was amplified by PCR using primers for hypervariable region 3–4 (V3–V4) of the 16S rRNA gene (515F and 907R). The PCR products was mixed and purified with GeneJET Gel Extraction Kit (Thermo Scientific). Then, sequencing libraries were generated and sequenced on an Illumina MiSeq platform and 250bp/300bp paired-end reads were generated. The UPARSE software package (provided in the public domain, http://www.drive5.com/usearch/) using the UPARSE-OTU and UPARSE-OTUref algorithms were performed for sequence analysis. The sequences with $\geq$ 97% similarity were assigned to the same OTUs. We selected a representative sequence for each OTU and use an RDP classifier to label the classification information for each representative sequence.

LC-MS analysis

30 mg feces was weighed, and 300 mL of pre-cooled ultrapure water was added for homogenizing treatment. 500 μl of precooled methanol and 10 μl of internal standard was added to 100 μl feces homogenate or serum, which was then mixed with a vortex and incubated at −20°C for 20 min. Then the samples were centrifuged at 14000 g for 15 minutes. The supernatant (400 μl) was taken for vacuum drying and 100 uL methanol-water (1:1, v/v) was added to dissolve the residue which was then centrifuged again at 14000 g for 15min.

The molecules in the supernatant were separated with a Waters ACQUITY UPLC i-class system (Waters, MA, USA). Mobile phase: phase A is 0.1% formic acid, and phase B is methanol. The sample (2 μl) was placed in an automatic sampler at 8°C, with a column temperature of 45°C and a flow rate of 300 ul /min. The liquid phase gradient was used as follows: from 0 to 6 min, B phase changing linearly from 60% to 65%. At 6-13 min, the B phase changed linearly from 65% to 80%. During 13-13.5 min, the B phase changed linearly from 80% to 90%. From 13.5 to 15min, the phase B was maintained at 90%. The 5500 QTRAP mass spectrometer (AB SCIEX) was used for mass spectrometry analysis in the anion mode.

Gut colonization with *Clostridium scindens*

C57BL/6j mice were given an antibiotics treatment to deplete the gut flora as previously described (Dapito et al., 2012) using drinking water containing four antibiotics with 1 g/L neomycin, 1 g/L ampicillin, 1 g/L metronidazole and 0.5 g/L vancomycin (Sigma-Aldrich, MO, USA). Seven days later, the antibiotic mixture was stopped, and the mice were given an oral gavage of vehicle (anaerobic glycerol) or 10^9 *C. scindens* every day for 7 days. *C. scindens* was purchased from American Type Culture Collection (ATCC35704, MD, USA), and grown under anaerobic conditions. Seven days after gavage, real-time PCR was performed using primers specific for *C. scindens* to confirm the colonization with *C. scindens*. EAU was subsequently induced after colonization as described above.

Real-time PCR

Total RNA was extracted from cells by using the TRIzol Reagent (Invitrogen, CA, USA). The PrimeScript RT reagent Kit (Takara, Dalian, China) was used to generate cDNA. Real-time PCR was performed with the ABI Prism 7500 system (Applied Biosystems, CA, USA) by using the iTaq Universal SYBR Green Supermix (BIO-RAD, CA, USA). The primer sequences are listed in Key resources table. Relative mRNA expression was calculated with the $2^{-\Delta\Delta ct}$ method.

Cell culture

Bone-marrow dendritic cells were collected and cultured as described (Lutz et al., 1999). Bone marrow cells were cultured in RPMI 1640 medium supplemented with 10% FBS, 1% penicillin/streptomycin, 20 ng/mL granulocyte-macrophage colony-stimulating factor (GM-CSF, R&D Systems, USA) and 10 ng/mL IL-4 (R&D Systems) to generate BMDCs. On day 10, $5*10^5$ BMDCs were plated in a 48-well plate and stimulated with lipopolysaccharide (LPS, 1 μg/mL, Sigma-Aldrich) and DCA (80uM, Sigma-Aldrich, MO, USA) or INT-777 (100uM, MedChem Express, USA) for 24h, whereafter the cells and supernatant were collected for further analysis. For co-cultured study, BMDCs were treated with 10ug/ml $IRBP_{651-670}$ for 24 hours before primed by LPS.

Mouse naive $CD4^+$T cells from EAU mice were isolated by mouse Naive CD4+T Cell Iso Kit (Miltenyi Biotec, Bergisch Gladbach, Germany) and co-cultured with DCA or INT-777 pretreated BMDCs (or vehicle) at a $CD4^+$T cells: BMDCs ratio of 5:1 for 5 days. Cells and supernatant were then collected for further analysis.

Human $CD14^+$ monocytes isolated from peripheral blood mononuclear cells of healthy donors, BD patients and VKH patients were purified by human CD14 microbeads (Miltenyi Biotec). $CD14^+$ monocytes cells were cultured in RPMI 1640 medium containing GM-CSF (100 ng/mL; AcroBiosystems, Newark, NJ, USA) and IL-4 (50 ng/mL; AcroBiosystems) to generate DCs. On day 7, $5*10^5$ DCs were plated in a 48-well plate and stimulated with 100 ng/ml LPS and DCA (80uM) or INT-777 (100uM) for 24h. Then the cells and supernatants were collected for further analysis.

Hematoxylin and eosin (H&E) staining

Mouse eyeballs were dissected and fixed with paraformaldehyde. Eyes were then washed, dehydrated and embedded in paraffin wax. Serial 6 μm sections were cut through the cornea-optic nerve axis, stained with H&E and scored according to Caspi's criteria (Agarwal et al., 2012).

Flow cytometry

For IL-17 and IFN-γ staining, cultured CD4+T cells were stimulated with PMA (50ng/mL) and ionomycin (1g/mL) for 1 hour at 37°C, brefeldin A (Sigma-Aldrich) for another 4 hours, then washed, fixed and permeabilized. Fluorescent anti-mouse CD4-APC, anti-mouse IL-17A-PE, anti-mouse IFN-γ-PE-cy7, anti-mouse CD25-PE, anti-mouse foxp3-PE-cy7, anti-mouse CD11c-APC, anti-mouse MHCII-PE and anti-mouse IgG isotype were purchased from eBiosciences. The following markers were used to identify different immune cell subsets: $CD11c^+MHCII^{high}$ for DCs, CD4+CD25+foxp3+ for Treg, CD4+IFN-γ+ for Th1, CD4+IL-17A+ for Th17 cells.

Cultured BMDCs or human MO-DCs were stained with anti-mouse CD80 (PE, eBioscience), CD86 (FITC, eBioscience), CD40 (FITC, BioLegend) and MHCII molecules (PE, eBioscience) or anti-human CD80 (PE, BioLegend, San Diego, CA, USA), CD86 (PE-cy7, BioLegend), HLA-DR (PE-cy5.5, BioLegend) and CD40 (FITC, BioLegend) at 4°C for 30 minutes.

Western blot

Lysates extracted from tissues and cultured cells were separated by SDS-PAGE and proteins were transferred to PVDF membranes. Membranes were incubated after blocking with 5% milk by using the following primary antibodies: TGR5 (1:1000, Abcam), P65 (1:1000, Abcam), phospho-P65 (1:2000, CST), Ikbα (1:1000, Abcam), phospho-Ikbα (1:10000, Abcam), CREB (1:2000, Abcam), phospho-CREB (1:2000, Abcam), beta-actin (1:2000, Abcam) at 4°C overnight. Membranes were then washed and incubated with secondary antibodies at room temperature. The membranes were visualized by Western Bright™ ECL kit (Advansta, CA, USA).

QUANTIFICATION AND STATISTICAL ANALYSIS

Bacterial community analysis

To calculate α diversity, we simplified the OTU table and calculated three indicators: Chao1 estimates the species richness; Observed Species estimates the amount of unique OTUs found in each sample, and Shannon index. Before cluster analysis, principal component analysis (PCA) was used to reduce the dimension of the original variables using the QIIME software package (Caporaso et al., 2010). QIIME calculates both weighted and unweighted unifrac distance, which are phylogenetic measures of β diversity. We used unweighted unifrac distance for Principal Coordinate Analysis (PCoA) and Unweighted Pair Group Method with Arithmetic mean (UPGMA) Clustering.

The linear discriminant analysis (LDA) of effect size (LEfSe), which was performed by the LEfSe tool (provided in the public domain, http://huttenhower.sph.harvard.edu/lefse/) was used to confirm differences in the abundances of individual taxonomy between the two groups. Only those taxa that showed a log LDA score > 2 and a P value < 0.05 were ultimately considered.

Statistical analysis

Results are shown as mean ± standard deviation (SD). One-way ANOVA and Kruskal–Wallis test were used to perform multiple group comparisons followed by Dunn's correction. Paired-samples t test and Wilcoxon test were used to analyze paired samples. Unpaired t test and Mann–Whitney U test were used to analyze two independent groups. Statistical analyses were performed with SPSS version 22.0 statistical software (SPSS, Chicago, IL, USA) and GraphPad Prism 7 software (GraphPad Software, Inc, CA). Data were considered significant when $p < 0.05$.